Nanowire morphology

DOI: 10.1002/smll.200600503

Growth Mechanism of Truncated Triangular III–V Nanowires**

Jin Zou, Mohanchand Paladugu, Hui Wang, Graeme J. Auchterlonie, Ya-Nan Guo, Yong Kim, Qiang Gao, Hannah J. Joyce, H. Hoe Tan, and Chennupati Jagadish*

Metal–organic chemical vapor deposition (MOCVD) techniques have been widely used to synthesize III–V semiconductor nanowires with Au colloidal nanoparticles acting as nucleation sites for nanowire growth. For III–V semiconductor nanowires grown on {111}B surfaces, tapered nanowires have been frequently observed. In this study, structural characteristics of tapered GaAs nanowires grown on the {111}B GaAs surface were investigated using electron microscopy. Detailed structural analysis suggests that the cross sections of the lower section of the tapered GaAs nanowires are truncated triangles. The formation mechanism of such structural characteristics is uniquely determined and discussed.

Growth of semiconductor nanowires has been of current research focus due to their scientific importance and potential technological applications in nanoelectronics and -optoelectronics.[1] Since electronic and optical properties of nanowires are very sensitive to their morphologies, it is critical to understand the relationship between the structural characteristics of semiconductor nanowires and their growth behavior in order to design and manufacture semiconductor nanowires with desired properties. Currently, semiconductor nanowires are commonly grown by chemical vapor deposition (CVD),[2] metal–organic chemical vapor deposition (MOCVD),[3] molecular beam epitaxy (MBE),[4] and chemical beam epitaxy (CBE).[5] The most widely reported growth mechanism for these semiconductor nanowires is the vapor–liquid–solid (VLS) growth mechanism, firstly proposed by Wagner and Ellis for the growth of Si whiskers decades ago.[6] In the VLS process, the directional growth is mainly induced and controlled by the liquid alloy droplets formed at the semiconductor–metal interface. The diameter of a nanowire at the growth front is generally limited by the size of the liquid alloy droplets. However, unusual morphologies of nanowires such as kinked nanowires,[7] branched nanowires,[8] nanowire sidewall faceting,[9] and nanowire tapering[10] have been often observed, indicating that there might exist other mechanisms affecting the morphology of nanowires. Givargizov[11] described the periodic diameter oscillation of Si whiskers grown by the VLS mechanism and suggested that this was attributed to the surface-energy modulations for growing submicrometer-sized whiskers in which the Gibbs–Thompson effect should be taken into account. Using in situ electron microscopy, Ross et al.[12] observed the sidewall faceting in Si nanowires and interpreted the phenomenon as an interplay between the geometry and surface energies of the nanowires and the shape of the liquid alloy droplet. Hiruma et al.[13] found two different growth models based on the VLS mechanism to describe the relationship between the growth rate and the width of III–V nanowires grown by MOCVD at two different temperature regimes. Nanowires grown at a higher temperature and a longer time were found to be tapered in shape, with a wider base in contact with the substrate and a narrower top.[13,14] Recently, a diffusion-controlled vapor–solid (VS) process of lateral growth was suggested to explain the tapering of heterostructured nanowires grown at higher temperatures using MOCVD.[15]

MOCVD is a well-established technique for the growth of epitaxial III–V semiconductor layers. It has also been widely used for growing high-quality III–V nanowires through the VLS mechanism, in which nanosized metal catalysts, usually Au particles, are commonly used to initiate the VLS growth.[16] In a typical process, single-crystalline wafers with deposited Au nanoparticles are placed in a growth chamber and the nanowire growth is initiated by the flow of vapor reactants at the growth temperature. When grown on {111}B surfaces, III–V semiconductors of zinc blende structures tend to grow vertically oriented in the $<111>$B direction.[10]

It has been shown that compound semiconductor nanowires with the zinc blende structure (such as GaP) exhibit intriguing morphological features.[17] According to crystallography, the zinc blende structure possesses polarity, leading to [u, v, w] $\neq$ [$\bar{u}$, $\bar{v}$, $\bar{w}$] and (h, k, l) $\neq$ ($\bar{h}$, $\bar{k}$, $\bar{l}$). As a consequence, compound semiconductor nanowires with the zinc blende structure exhibit more complicated morphologies than the elemental semiconductor nanowires, which, in turn, might result in different electronic and optoelectronic properties. In this paper, the detailed morphological and structural features of GaAs nanowires grown by MOCVD on (111)B GaAs substrates are investigated using electron microscopy and the underlying formation mechanism is exclusively determined.

GaAs nanowires were grown on a {111}B GaAs substrate in a horizontal-flow MOCVD reactor at a pressure of 100 mbar. The total flow rate of H_2 carrier gas in the reactor

[*] Dr. J. Zou, M. Paladugu, Dr. H. Wang, G. J. Auchterlonie, Y.-N. Guo
School of Engineering and
Centre for Microscopy and Microanalysis
The University of Queensland
QLD 4072 (Australia)
Fax: (+61) 7-3365-3888
E-mail: j.zou@uq.edu.au
Prof. Y. Kim, Dr. Q. Gao, H. J. Joyce, Dr. H. Hoe Tan,
Prof. C. Jagadish
Department of Electronic Material Engineering
Research School of Physical Sciences and Engineering
The Australian National University
Canberra, ACT 0200 (Australia)
Prof. Y. Kim
Department of Physics, Dong-A University
Hadan-2-dong, Sahagu, Busan 604-714 (Korea)

[**] This research is supported by Australian Research Council. The authors would like to acknowledge the useful comments of Prof. David Cockayne.

cell was 1500 sccm (sccm = standard cubic centimeters per minute). Prior to nanowire growth, the substrate with Au nanoparticles was annealed in situ at 600 °C under AsH_3 ambient for 10 min to desorb surface contaminants and to form a eutectic alloy between nanosized Au particles and Ga from the substrate. After cooling to the desired growth temperature, group III source gases were switched on to initiate the nanowire growth. The molar flow rates of trimethylgallium (TMG) and AsH_3 were 1.2×10^{-5} mol min^{-1} and 5.4×10^{-4} mol min^{-1}, respectively. A growth temperature 450 °C was determined to be the optimum temperature, based on a number of experiments. To grow nanowires with sufficient length, a growth time of 30 min was used for all GaAs nanowire growth.

Detailed morphology and structure of grown GaAs nanowires was characterized by high-resolution scanning electron microscopy (HR-SEM; JEOL JSM 890 with a cold FEG) and transmission electron microscopy (TEM; FEI Tecnai F30). TEM specimens were prepared by ultrasonicating a solution containing nanowires in ethanol for 20 min and then dispersing the nanowires onto holey carbon films.

Extensive SEM observations showed that most of the GaAs nanowires were freestanding and have a tapered shape with a thin apex and a thick base. All the nanowires grew perpendicular to the substrate surface, that is, along the $[\bar{1}\bar{1}\bar{1}]$ direction, if the substrate surface is taken as $(\bar{1}\bar{1}\bar{1})$ (one of the (111)B surfaces). Figure 1a shows a typical SEM image taken with the substrate normal tilted 30° from the electron beam, with all the GaAs nanowires showing the tapered shape. In order to see their detailed surface morphology, an extensive SEM study (viewed in different directions and focused in different regions) of individual nanowires was carried out. Figure 1b and c shows a pair of SEM images taken from a typical nanowire (focused on the lower region of the nanowire) with the substrate normal tilted 0° and 10° from the electron beam, respectively. As can be seen from Figure 1b (the nanowire was parallel to the electron beam), two truncated triangles overlap with a rotation of $n\times60°$ (n = integer) to each other. Interestingly, when the nanowires were titled away from the electron beam (Figure 1c), a number of overlapping truncated triangles, organized in two orientations – rotated by $n\times60°$, was observed. This observation suggests that the cross section in the lower region of the GaAs nanowires has the truncated triangular shape. To understand the surface morphology of the sidewalls of these GaAs nanowires and how the truncated triangular cross section is formed, SEM images focused on different regions of a nanowire were captured. Figure 1d and its inset show a pair of SEM images focused on the lower and top regions, respectively, in which the nanowire was slightly titled away from the electron beam (<5°). It is of interest to note that, unlike the truncated triangular shape, the top region of the nanowire (inset in Figure 1d) shows distinct hexagonal faceted sidewalls under the Au catalyst particle (shown as a darker circle). The width of the hexagon is close to the diameter of the Au particle. The comparison of Figure 1d and its inset suggests that the faceted crystal planes of the hexagon sidewalls are parallel to the long edge of the truncated triangles. This suggests that the formation of truncated triangular cross section in the lower region of the GaAs nanowires is due to a lateral growth occurring simultaneously with the axial nanowire growth.

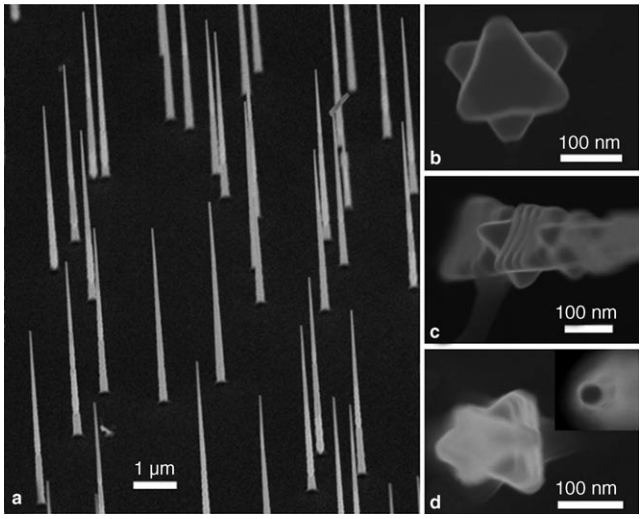

Figure 1. SEM images of GaAs nanowires: a) A low-magnification image showing the tapered nanowires; b, c) top and 10°-tilted views of a nanowire showing it to have a truncated triangular cross section and overlapping truncated triangles; d) a slightly tilted view of a nanowire focused on the lower region and, in the inset, focus on the top region.

Although distinct facets of GaAs nanowires can be clearly seen from the HR-SEM images at both the top and lower regions, it is not possible to determine the crystallographic planes of these sidewall facets from SEM images. For this reason, detailed TEM characterization was carried out. Individual nanowires were collected on holey carbon films for observation by TEM. The $[\bar{1}\bar{1}\bar{1}]$ growth direction of each nanowire could be determined from the fact that the nanowire tapers as it grows (see Figure 1a). By using selected-area electron diffraction (SAED) to align the nanowires to a particular zone axis, on-zone bright-field TEM images were taken from a lower section of a GaAs nanowire that contained several segments (marked as Γ or Λ in Figure 2a–c). These on-zone TEM images were taken along two <110> directions (Figure 2a and c) and one <112> direction (Figure 2b), each tilted 30° away from its adjacent one, as indicated in Figure 2d. As can be clearly seen, the two <110> on-zone TEM images show asymmetric projected morphology for each nanowire segment, that is, one side is relatively smooth while the other side shows nonperiodic saw-tooth faceting, but the features in Figure 2a and c are opposite to each other (i.e., where the nanowire in Figure 2a is smooth, the nanowire in Figure 2c shows nonperiodic saw-tooth faceting, and vice versa). Furthermore, the two adjacent segments (such as Γ and Λ) have opposite projected morphology in each of Figure 2a and c.

By combining these results with SEM observations, the truncated triangular nature of the cross section in the lower sections of nanowires and the rotation of adjacent triangular segments are clearly confirmed. These two structural characteristics are illustrated in Figure 2d. Based on crystallog-

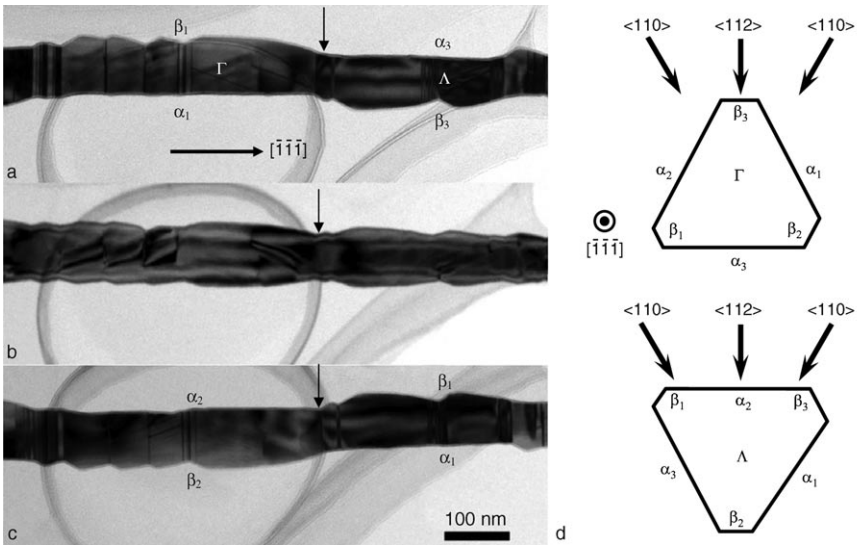

Figure 2. TEM bright-field images on different zone axes of a lower section of a typical GaAs nanowire: a, c) $<110>$; b) $<112>$; d) a schematic diagram showing the growth direction and two cross sections of rotated truncated triangular segments. The TEM viewing directions are indicated and corresponding projections (α_i and β_i) are shown in (a) and (c).

raphy, the six edges of a truncated triangle shown in Figure 2d are the projections of the six {112} crystal planes (perpendicular to the $[\bar{1}\bar{1}\bar{1}]$ growth direction) along the growth direction. Considering the possible side projections of a three-dimensional nanowire suggests that the longer edges of a given truncated triangle, α_i (i = 1, 2, and 3) correspond to the smooth sides shown in Figure 2a and c. The fact that the short edges β_i correspond to nonsmooth edges when viewed along different $<110>$ directions indicates that the length of β_i varies along the growth direction, which, in turn, causes variations of α_i. Although the variation of the length of the long edges cannot be identified in the $<110>$-projected TEM images, Figure 2b confirms such variations through both nonsmooth projected edges. Moreover, the necked morphology is associated either with the boundary of two adjacent segments (marked as an arrow in Figure 2a–c) or with the concave facet of each saw tooth in the $<112>$-projected TEM images.

It is of interest to note that at least one planar defect (shown as dark lines) is associated with the concave facet of each saw tooth or the boundary between adjacent triangular segments. To determine their structural nature at the atomic level, high-resolution TEM (HRTEM) investigations were carried out. Figure 3a is a bright-field TEM image viewed along a $<110>$ zone axis and shows the faceted saw tooth and a segment boundary. Figure 3b and c present HRTEM images taken from a boundary region and a concave region, respectively, both showing twinned structures. The planar defect in the boundary showed a thin multiply twinned structure resulting in an overall twin, while that in the concave region is a thin twin structure (only four atomic monolayers thick) inserted into a perfect crystal region. According to crystallography, twins on {111} crystal planes in the zinc blende structure can only be formed by rotation with possible rotations of $n \times 60^\circ$ due to the …AaBbCcAaBbCc… stacking sequence along $<111>$.[18] As a consequence, the twinned structures shown in the HRTEM images indicate that the adjacent segments Γ and Λ must be related by rotation twins along the $[\bar{1}\bar{1}\bar{1}]$ growth direction, which fits well with all of the SEM and TEM observations.

Since the polarity in the zinc blende structure leads to $(h, k, l) \neq (\bar{h}, \bar{k}, \bar{l})$, the six {112} sidewalls are not all equivalent. In fact, they can be crystallographically classified as {112}A (with two threefold-coordinated group III surface atoms and one twofold-coordinated group V atom in each

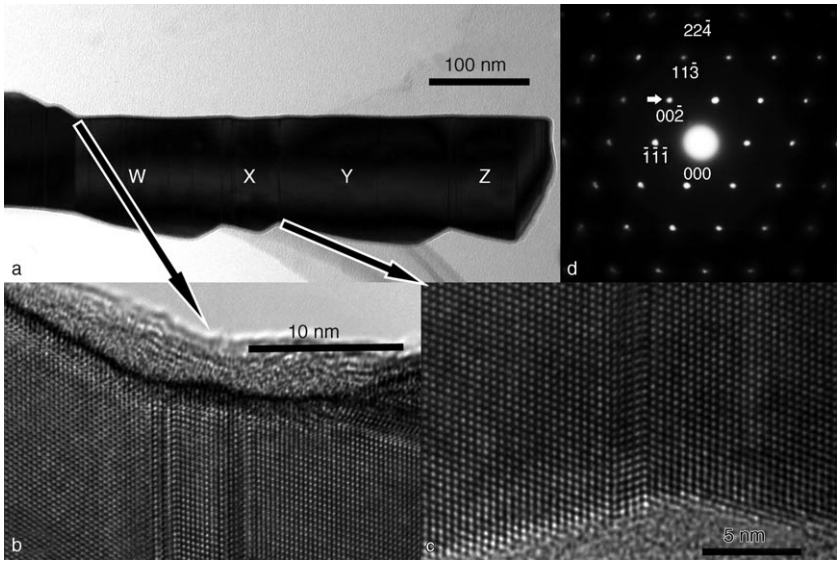

Figure 3. a) a bright-field TEM image taken from a lower region of a GaAs nanowire with corresponding high-resolution TEM images (b and c) taken from the boundary of two adjacent segments and the concave (as marked by arrows); d) a SAED pattern that corresponds to (a).

surface unit cell) and {112}B (with two threefold-coordinated group V surface atoms and one twofold-coordinated group III atom in each surface unit cell).[19] According to crystallography, all the α_i planes shown in Figure 2d are equivalent and similarly for β_i. To distinguish whether α_i or β_i belong to {112}A or {112}B, SAED was employed. Figure 3d is a SAED pattern taken from the nanowire shown in Figure 3a. The {111}*-type reflection, which is in the growth direction, is designated $(\bar{1}\bar{1}\bar{1})$* to be in agreement with the $[\bar{1}\bar{1}\bar{1}]$ growth direction. As can be seen from Figure 3d, there is a {200}* type of reflection (marked by an arrow) that has an acute angle with $(\bar{1}\bar{1}\bar{1})$*, indicating that, as required crystallographically, it must be one of the $(00\bar{2})$*, $(0\bar{2}0)$*, or $(\bar{2}00)$* reflections. Since these three reflections are equivalent in the zinc blende structure and their arbitrary choice would not cause any change of the nature of the {112} planes, we can index the reflection as $(00\bar{2})$* for the convenience of further discussion. In turn, other reflections can be indexed (some of them are shown in Figure 3d) and the zone axis of the diffraction pattern can be determined to be $[\bar{1}10]$.

To understand how the surface morphology evolves during the lateral growth, we need to examine the atomic structure of the nanowire within the growth environment. Figure 4a shows an atomic structure along the $[\bar{1}10]$ projection, that corresponds to the SAED pattern of the main segment of the nanowire shown in Figure 3a. It is important to note that 1) the Ga and As atoms cannot be interchanged in this model because the $(\bar{1}\bar{1}\bar{1})$ growth surface at the right-hand side presents this, and 2) the model shown in Figure 4a cannot be twinned or rotated along the $[\bar{1}\bar{1}\bar{1}]$ direction because the observed SAED pattern prevents this. This structural analysis suggests that the smooth {112} surface shown in Figure 3a is the $(11\bar{2})$ plane (as it is perpendicular to the $[22\bar{4}]$* direction). From Figure 4a and the crystallographic definition, this smooth {112} surface belongs to {112}B and its opposite non-smooth {112} surface is the $(\bar{1}\bar{1}2)$ plane, which belongs to {112}A.

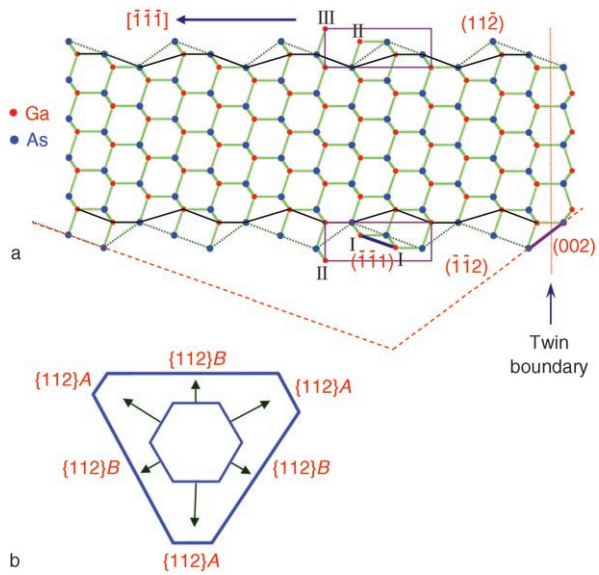

Figure 4. Schematic diagrams of a) a $[\bar{1}10]$-projected GaAs atomic structure and b) a truncated triangle transition from a hexagonal cross section due to differential lateral growth along different {112} sidewall surfaces.

The projections of ideal $(11\bar{2})$ and $(\bar{1}\bar{1}2)$ surfaces are shown by solid black lines. As can be seen from the growth parameters outlined earlier, the concentration of the As species is over 40-times higher than that of the Ga species in order to maintain effective axial growth. Because of this, every surface Ga atom exposed in this environment would be rapidly bonded with As atom(s) depending on how many broken bonds are available. This leads to new semiequilibrium {112} sidewall surfaces (i.e., covered entirely by As atoms) as indicated by the dotted green lines. Under such an As-rich environment, if a Ga atom is available for the lateral growth, the question now is which Ga position would be occupied in the semiequilibrium {112} surfaces, that is, $(11\bar{2})$ or $(\bar{1}\bar{1}2)$? To answer this question, we can draw $<110>$-projected {112} surface unit cells (as indicated by the purple rectangular boxes) to study these possible occupation sites. All possible Ga-incorporating sites are marked by Roman numerals. The five positions can be classified into three groups, marked as I, II, and III. Each Ga atom in the type I position is threefold-coordinated,[19] while for the type II and III positions, each Ga atom is twofold- and singly coordinated, respectively. This indicates that each Ga atom in the type I position can recover three broken bonds with three neighboring As surface atoms, while for the type II and III positions, each Ga atom can only recover two and one broken bonds, suggesting clearly that it is most energetically favorable for Ga atoms to occupy type I positions during the lateral growth process. The fact that the two type I positions are on the {112}A surface implies that lateral growth would be predominantly along the $<112>$A directions.

It is of interest to note that the two type I positions in the $(\bar{1}\bar{1}2)$ surface unit cell form a $(\bar{1}\bar{1}1)$ atomic plane, as shown by a blue line in Figure 4a. This implies that the lateral growth along the $<112>$A direction actually takes place on their associated {111} planes. Since the concave facet of a saw tooth corresponds to a thin rotation twin, such a twin structure holds back the lateral growth (as marked by the vertical red dotted line), leaving a terminating {002} crystal plane, as indicated by the purple solid line. Based on this model, for a slice between two twinned structures (i.e., the slice of W or X shown in Figure 3a), a V-shaped projection (as marked as red broken lines in Figure 4a) that corresponds to $(\bar{1}\bar{1}1)$ and (002) atomic planes is expected if sufficient growth is allowed. This can be seen from Figure 3a that, for a thin slice (e.g., X), a well-defined V-shape can be seen, indicating the lateral growth is almost complete. While for the thicker slice (such as W or Y), the V shape is only partially fitted at both top corners, indicating that the lateral growth is not sufficient to cover the entire V shape for these slices. Since the saw-tooth faceting is controlled by the rotation twins and the twinning takes place randomly, the saw-tooth faceting is not periodic in our case, and is thus different from the periodic saw-tooth faceting observed in Si nanowires.[12]

If the lateral growth takes place only on the {112}A surface, it is expected that the size of the truncated triangles would be restricted by the size of catalyst nanoparticles. However, careful analysis of Figure 1d shows that the size of the truncated triangle is much larger than that of the hexagon in the top region of the nanowire, indicating that the lateral growth should also take place on the {112}B surfaces. Since the type II positions on the {112}B surface are the preferred lattice sites for Ga atoms and since, once a Ga atom occupies such a position, two As atoms would follow to cover the surface, it is crystallographically anticipated that, unlike the case of {112}A, the lateral growth should be uniformly developed on the {112}B surfaces, which is in excellent agreement with TEM observations.

Based on the above discussion, a lateral growth model can be proposed as follows, and the cross section is illustrated in Figure 4b. The hexagon-shaped sidewalls are {112} atomic planes with three of them belonging to {112}A and the other three belonging to {112}B in the zinc blende structure; since they are not equivalent, the imbalanced cations and anions available in the growth environment resulted in an asymmetric lateral growth. According to the analysis outlined above, the lateral growth on {112}A sidewalls is faster than that on {112}B sidewalls. Due to the nonplanar nature of {112} surfaces (refer to Figure 4a), the growth on {112}A sidewalls is preferential to the associated {111} atomic planes. Furthermore, since the rotation twins in GaAs need very little energy,[20] rotation twins can be seen frequently in GaAs. Due to the nature of {112} sidewall swaps (between A and B) by a rotation of $n \times 60^\circ$ along the $[\bar{1}\bar{1}\bar{1}]$ growth direction for a twin boundary, a rotation of the triangular shape by $n \times 60^\circ$ along the $[\bar{1}\bar{1}\bar{1}]$ growth direction is expected, which explains the alternating triangles seen in the SEM images (refer to Figure 1). If a thin twined structure is inserted in a perfect crystal region (refer to Figure 3c), this twinned structure would act to self-limit the growth through growth termination at the {111} and {002} atomic planes on the associated {112}A sidewalls (refer to the V shapes in Figure 3a and Figure 4a). Simultaneously, the lateral growth on the {112}B sidewalls is uniformly developed, leaving the {112}B sidewalls smooth.

In conclusion, the fundamental mechanism for the tapered morphology of GaAs nanowires grown by MOCVD has been determined through detailed electron microscopic investigation.

Keywords:
electron microscopy · indium · materials science · nanowires · semiconductors

[1] a) P. D. Yang, *MRS Bull.* **2005**, *30*, 85–91; b) Y. Huang, X. F. Duan, C. M. Lieber, *Small* **2005**, *1*, 142–147.
[2] Y. Wu, Y. Cui, L. Huynh, C. J. Barrelet, D. C. Bell, C. M. Lieber, *Nano Lett.* **2004**, *4*, 433–436.
[3] W. Seifert, M. Borgstrom, K. Deppert, K. A. Dick, J. Johansson, M. W. Larsson, T. Martensson, N. Skold, C. P. T. Svensson, B. A. Wacaser, L. R. Wallenberg, L. Samuelson, *J. Cryst. Growth* **2004**, *272*, 211–220.
[4] S. K. Chan, Y. Cai, I. K. Sou, N. Wang, *J. Cryst. Growth* **2005**, *278*, 146–150.
[5] B. J. Ohlsson, M. T. Bjork, M. H. Magnusson, K. Deppert, L. Samuelson, L. R. Wallenberg, *Appl. Phys. Lett.* **2001**, *79*, 3335–3337.
[6] R. S. Wagner, W. C. Ellis, *Appl. Phys. Lett.* **1964**, *4*, 89–90.
[7] J. Westwater, D. P. Gosain, S. Tomiya, S. Usui, H. Ruda, *J. Vac. Sci. Technol. A* **1997**, *15*, 554–557.
[8] Z. H. Wu, X. Mei, D. Kim, M. Blumin, H. E. Ruda, J. Q. Liu, K. L. Kavanagh, *Appl. Phys. Lett.* **2003**, *83*, 3368–3370.
[9] J. Johansson, B. A. Wacaser, K. A. Dick, W. Seifert, *Nanotechnology* **2006**, *17*, S355–S361.
[10] K. Hiruma, M. Yazawa, K. Haraguchi, K. Ogawa, T. Katsuyama, M. Koguchi, H. Kakibayashi, *J. Appl. Phys.* **1993**, *74*, 3162–3171.
[11] E. I. Givargizov, *J. Cryst. Growth* **1973**, *20*, 217–226.
[12] F. M. Ross, J. Tersoff, M. C. Reuter, *Phys. Rev. Lett.* **2005**, *95*, 146104.
[13] K. Haraguchi, K. Hiruma, M. Yazawa, T. Katsuyama, *J. Electrochem. Soc.* **2006**, *153*, C1–C5.
[14] K. Hiruma, K. Haraguchi, M. Yazawa, Y. Madokoro, T. Katsuyama, *Nanotechnology* **2006**, *17*, S369–S375.
[15] a) M. A. Verheijen, G. Immink, T. de Smet, M. T. Borgstrom, E. Bakkers, *J. Am. Chem. Soc.* **2006**, *128*, 1353–1359; b) Y. Kim, H. J. Joyce, O. Gao, H. H. Tan, C. Jagadish, M. Paladugu, J. Zou, A. A. Suvorova, *Nano Lett.* **2006**, *6*, 599–604.
[16] Y. N. Guo, J. Zou, M. Paladugu, H. Wang, Q. Gao, H. H. Tan, C. Jagadish, *Appl. Phys. Lett.* **2006**, *89*, 231917.
[17] J. Johansson, L. S. Karlsson, C. P. T. Svensson, T. Martensson, B. A. Wacaser, K. Deppert, L. Samuelson, W. Seifert, *Nat. Mater.* **2006**, *5*, 574–580.
[18] a) D. B. Holt, *J. Mater. Sci.* **1984**, *19*, 439–446; b) A. Kelly, G. W. Groves, P. Kidd, *Crystallography and Crystal Defects*, Wiley, Chichester, **2000**, pp. 321–324.
[19] D. J. Chadi, *J. Vac. Sci. Technol. A* **1985**, *3*, 1167–1169.
[20] D. T. J. Hurle, P. Rudolph, *J. Cryst. Growth* **2004**, *264*, 550–564.

Received: September 20, 2006
Published online on February 6, 2007

